ISC-1176
PHYSICS

HALL COEFFICIENT AND RESISTIVITY OF A Mg_2Si SINGLE CRYSTAL FROM 4^oK TO 300^oK

By

Donald Richard Zrudsky
G. C. Danielson

May 1959

Ames Laboratory
Iowa State College
Ames, Iowa

DISCLAIMER

This report was prepared as an account of work sponsored by an agency of the United States Government. Neither the United States Government nor any agency thereof, nor any of their employees, makes any warranty, express or implied, or assumes any legal liability or responsibility for the accuracy, completeness, or usefulness of any information, apparatus, product, or process disclosed, or represents that its use would not infringe privately owned rights. Reference herein to any specific commercial product, process, or service by trade name, trademark, manufacturer, or otherwise does not necessarily constitute or imply its endorsement, recommendation, or favoring by the United States Government or any agency thereof. The views and opinions of authors expressed herein do not necessarily state or reflect those of the United States Government or any agency thereof.

DISCLAIMER

Portions of this document may be illegible in electronic image products. Images are produced from the best available original document.

TABLE OF CONTENTS

		Page
	ABSTRACT	iv
I.	INTRODUCTION	1
	A. The Semiconductivity of Mg_2Si	1
	B. Previous Work	1
	C. Purpose of this Work	3
II.	EXPERIMENTAL PROCEDURE	5
	A. Preparation of Sample	5
	1. Growing the ingot	5
	2. The finished sample	6
	B. Apparatus	7
	1. Cryostat	7
	2. Sample holder	10
	3. Thermocouple	13
	4. Electrical circuit	14
	C. Electrical Measurements	16
	1. Form of the data	16
	2. Check of Hall voltage linearity with magnetic field	17
	3. Calculation of resistivity	18
	4. Calculation of Hall coefficient	19
	D. Errors	25
	1. Resistivity	25
	2. Hall coefficient	25
	3. Temperature	27
III.	ANALYSIS OF THE RESULTS	30
	A. Hall Coefficient	30
	B. Hall Mobility	33
	C. Impurity Level	35
	D. Impurity Compensation	39
IV.	LITERATURE CITED	41
V.	APPENDIX	43

HALL COEFFICIENT AND RESISTIVITY OF A Mg_2Si SINGLE CRYSTAL FROM 4^oK TO 300^oK*

Donald Richard Zrudsky and G. C. Danielson

ABSTRACT

The Hall coefficient and resistivity of an n-type single crystal of Mg_2Si with a room temperature carrier concentration of 3.5 $(10)^{17}$ cm^{-3} was measured from 4.2 to 300°K. The Hall coefficient reached a peak value of 220 cm^3/coulomb at a temperature of 17.4°K and a saturation value of 76 cm^3/coulomb below a temperature of about 7°K. The Hall mobility of the sample had a temperature dependence of $T^{-2.2}$ at high temperatures and a temperature dependence of $T^{+3.1}$ at low temperatures. The high temperature measurements confirmed, but added nothing new, to some of the work of Morris, Redin, and Danielson. The low temperature measurements suggest a donor impurity level at 0.0045 ev below the conduction band. All of the low temperature data seemed to agree self-consistently with a theory of weak impurity band conduction. On the basis of this theory, a crude estimate of the percentage of acceptor impurities compensated by donor impurities was found to be 50 ± 25 per cent.

---

*This report is based on an M. S. thesis by Donald Richard Zrudsky submitted May, 1959, to Iowa State College, Ames, Iowa. This work was done under contract with the Atomic Energy Commission.

I. INTRODUCTION

A. The Semiconductivity of Mg_2Si

When a charged particle is treated quantum-mechanically, it assumes all the aspects of a wave. Electrical conduction in a single crystal is one manifestation of this wave motion through the periodic potential of the crystal. The band theory of solids treats this conduction in detail, relating the carrier momentum to its energy as a function of the crystal structure. It predicts alternate bands of allowed and forbidden energies, due to the constructive and destructive interference of the periodic array.

Band theory predicts 2N states in each allowed energy band of a crystal, containing N primitive unit cells. The antifluorite structure of Mg_2Si, shown in Figure 1, has three atoms per unit primitive cell. The entire crystal therefore provides $(2\cdot2+1\cdot4)N = 8N$ valence electrons. These electrons will fill 4 energy bands, causing the compound to be either a semiconductor or an insulator.

B. Previous Work

Mg_2Si is a member of the Mg_2X family, where X = Si, Ge, Sn, or Pb. All are semiconductors except Mg_2Pb, which acts as a metal. Previous electrical measurements have been made on Mg_2Si as well as the remaining members of the family.

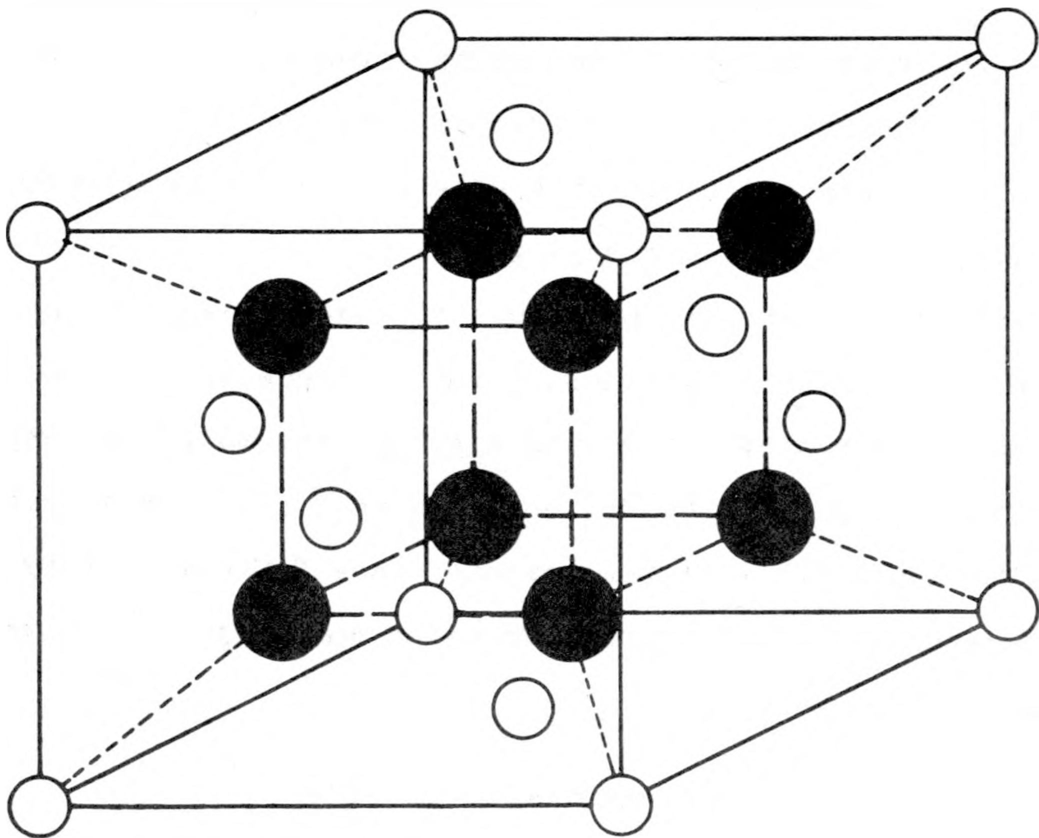

Figure 1. Unit cell of the fluorspar lattice; the blackened circles represent Mg and the blank circles represent Si

Properties of the whole series from 100°K to 1000°K, determined on the basis of thermoelectrical power, resistivity, and Hall coefficient of polycrystalline samples have been summarized by Winkler (15).

Whitsett (14) was the first to make electrical measurements on a single crystal of Mg_2Si from 60 to 1000°K. However, the most recent and comprehensive work on single crystals of Mg_2Si from 80 to 1000°K was done by Morris, _et al_. (11), who measured both n-and p-type single crystals ranging in saturation carrier concentration from $8(10)^{16}$ to $7(10)^{17}$ cm^{-3}. They arrived at a ratio of electron mobility to hole mobility of 4.8 and an energy gap of 0.78 ev. The electron mobility of the purest sample was fitted very well between 80 to 300°K by a combination of optical mode and ionized-impurity scattering. Frederikse, _et al_. (4) made low temperature measurements on Mg_2Sn, but because of their high purity samples and more reactive compound, they found what they considered a surface state phenomenon dominating their results.

C. Purpose of this Work

The purpose of this investigation was to measure the low temperature electrical properties of a Mg_2Si single crystal. It was hoped that an application of band theory

might establish the impurity energy level and to clarify further the carrier scattering mechanisms.

II. EXPERIMENTAL PROCEDURE

A. Preparation of Sample

1. Growing the ingot

Single crystals of Mg_2Si had been prepared prior to this investigation by Morris, *et al*. (11). Sublimed magnesium supplied by Dow Chemical Company, with a purity of 99.99 per cent or better, and Sylvania transistor-grade silicon were used. The magnesium was cleaned and rinsed before weighing. The silicon was not cleaned because it had been kept free of surface contamination. Stoichiometric proportions, two atoms of magnesium to one of silicon, were added to a crucible. The crucible had a spectrographically-pure graphite liner inside a 1 3/8-inch carbon cylinder 4 1/2 inches long. The crucible had previously been thoroughly cleaned and outgassed.

The crucible and contents were placed in a furnace and the pressure was reduced to $5(10)^{-5}$ mm Hg. Magnesium boils at 1107°C, while the compound melts at 1090°C. Since the vapor pressure of magnesium is nearly one atmosphere, 20-30 pounds gauge pressure of argon was admitted in order to retain the magnesium. The melting point of the compound was reached within an hour, after which a temperature gradient of about 25°C/cm was established. In order to establish this gradient, the furnace coils were raised and tap water was allowed to circulate through cooling coils attached to the

bottom of the chamber. The melt was solidified within an hour, and the ingot was then cooled 50°C/hour to room temperature. The temperature gradient allowed crystallization to start at one point and proceed slowly in one direction, thus increasing the probability of growing a single crystal. The slow cooling reduced regional differential expansions which might crack the crystal.

2. The finished sample

When the crucible was carefully chipped open the entire ingot area exposed to the crucible was found to be bonded to the graphite liner. The ingot was cleaved and samples from various portions of the ingot were first crudely shaped on a grinding wheel. The samples were then waxed to a microscope slide and shaped into a rectangular form by means of 400-mesh silicon carbide paper. In order to check the rectangular samples for homogeneity, the resistivity was measured at opposite ends of each side. The samples taken from the center of the ingot appeared to have the highest inhomogeneity. This inhomogeneity may have been caused by a loss of magnesium due to evaporation. Since the ingot cooled from the outside to the inside, the exact proportions of the constituents may have frozen to yield Mg_2Si at first, but as the cooling continued toward the center, silicon rich eutectic may have been frozen into the crystal.

The sample chosen for this work had the dimensions 0.855 mm x 1.217 mm x 4.960 mm. The maximum deviation of resistivity from the average along any of the longitudinal faces was 9 per cent. Laue back-reflection x-ray photographs had been made at three points along all the samples reported by Morris, *et al*. (11). Morris concluded that all the samples were either single crystals or consisted of a small number of slightly different orientations. Since the ingot from which the sample of this report was taken had been grown in a similar fashion and since it cleaved easily, it was assumed that it too was a single crystal.

After several attempts to measure the sample had failed, it was found necessary to make three tiny holes on the sides of the sample in which to rest the tungsten probes. In order to make these holes, a piece of masking tape with pin holes in it was put on the side of the sample. When an air abrasive probe was passed over the tape, the desired holes were produced in the sample at the location of the pin holes.

B. Apparatus

1. Cryostat

The construction of a cryostat suitable for the purpose of this research is illustrated in Figure 2. The cryostat was all metal, about four feet long and five inches in di-

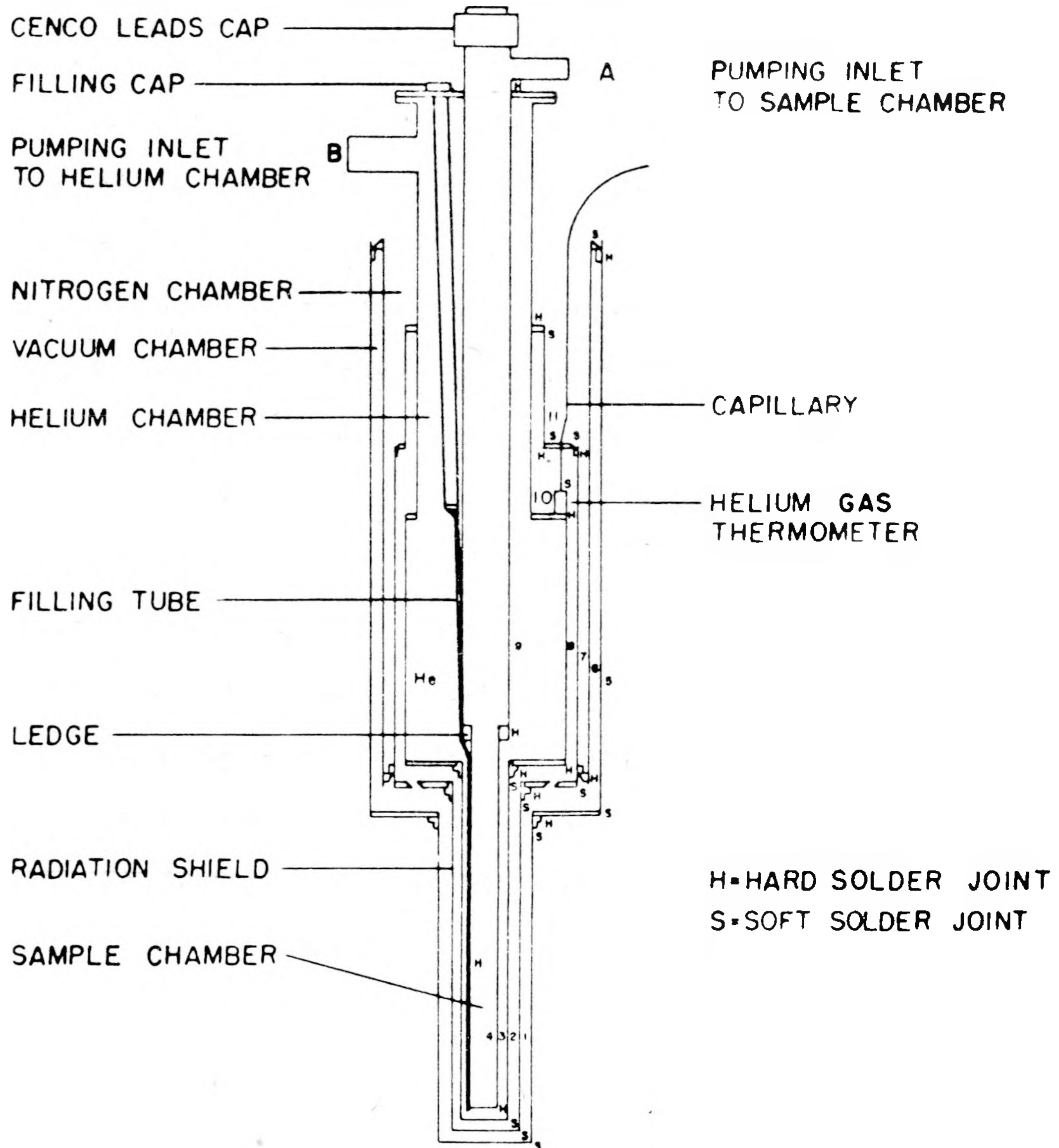

Figure 2. Liquid helium cryostat

ameter at the top. The bottom was provided with a tail two inches in diameter to fit between the pole pieces of a magnet. Construction was predominantly of copper or brass except where thermal conduction was to be kept to a minimum. Stainless steel or monel was used in these places. Hard and soft solder joints were alternated throughout the internal construction so that the cryostat could be taken apart.

Skew holes in the plate between the vacuum chambers provided coupling, but prevented radiation from warm to cold surfaces. Tubes 8 and 6, Figure 2, were wrapped with aluminum foil (shiny side out) to act as radiation shields. The tubes were then secured with fine wire. Extreme care had to be taken to avoid touching the surface with greasy hands, as the emissivity of organic materials is very high.

The fill-tube extended from the cryostat top to within 1/16 inch of the helium chamber bottom. Outlet B was provided in order that pressure could be applied to the liquid helium chamber and cause the liquid nitrogen pre-coolant to be transferred out of the fill-tube. Outlet B was also provided for pumping on the liquid helium. The sample chamber could be pumped out or transfer gas could be let in through outlet A. This pressure control, along with a heater wire wound around the sample holder, provided the means of temperature control.

A gas thermometer was soldered to the top of the helium chamber. When the thermometer was evacuated and filled with helium gas to a few pounds pressure, one could tell when the liquid helium level had reached this point, for the gas in the thermometer contracted greatly and the gauge reading fell to a low value. The helium chamber held 1.6 liters of liquid helium, which lasted about 15 hours. This time was usually sufficient to complete a run.

2. Sample holder

The sample was mounted in the sample holder shown in Figure 3. With the sample in place, a cylindrical can was slid over the holder and press fitted to the holder cap. The backing plate, can, and holder cap were all made of 99.999 per cent purity deoxidized copper which had a thermal conductivity at low temperatures 10 to 100 times the thermal conductivity of commercial grades of copper according to Chelton and Mann (2, p. 86). It was hoped that high conductivity materials would be less likely to sustain gradients and equilibrium would thus be reached sooner.

Electrical isolation of all probes from ground was accomplished by mounting two lucite blocks on the copper backing plate. A butt-end copper current probe could be bolted to the first lucite block. A spring loaded vise was fastened to the other lucite block to serve as the other current

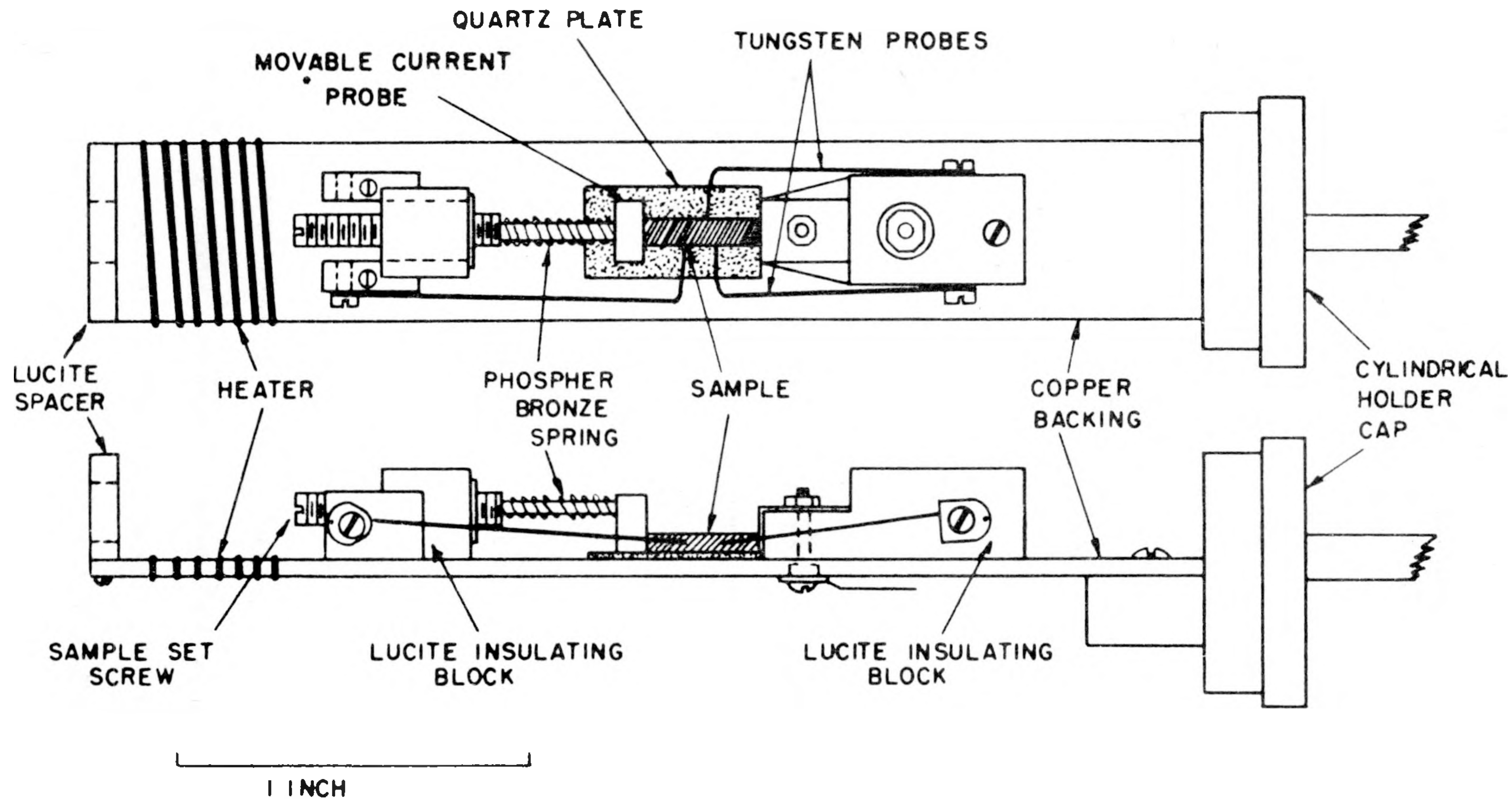

Figure 3. Low temperature sample holder

probe. Three tungsten potential probes were also bolted to the sides of the lucite blocks by means of brass inserts. The sample and movable current probe rested on a 0.010-inch thick quartz plate adhered to the backing plate with General Electric no. 7031 calorimeter varnish. Quartz was chosen because of its excellent insulating properties as well as its exceedingly high thermal conductivity at low temperatures ($K \cong 10$ W/cm °K at $T = 10$°K) (13). The quartz played a dominant role in dissipating the sample-power generated by the current passing through it, particularly when the transfer gas had been pumped from the chamber.

At the lowest end of the holder, four feet of 6 mil. constantan silk-wrapped wire was wound non-inductively on the backing plate to serve as a heater. A gold cobalt vs. copper thermocouple was cemented into thermal contact with the fixed current probe to serve as the only temperature measuring device.

Careful calculations were made to select the proper material and wire diameters for all the electrical leads. The goal was to minimize liquid helium consumption and yet maintain reasonable galvanometer sensitivity in the measuring circuits. Most materials which had low thermal conductivity also had high electrical resistivity, which increased I^2R losses and decreased the measuring sensitivity. Constantan was selected as the compromise material. Several inches of

each potential and thermocouple lead were wrapped around the upper end of the sample holder and thermally bonded to the sample holder by means of General Electric no. 7031 calorimeter varnish. This bonding prevented the undesirable thermal currents near the sample.

3. Thermocouple

As mentioned in the last section, a gold-cobalt versus copper thermocouple was cemented to the fixed current probe to serve as a temperature measuring device. This thermocouple is described in detail by Fuschillo (5). However, a calibration by Schirber[1] for this particular batch of thermocouple wire was used as the basis for the scale. The particular thermocouple used was calibrated several times directly in the cryostat at liquid helium and at liquid nitrogen temperatures. This thermocouple agreed quite closely with Schirber's data, measuring 20 microvolts lower at liquid helium temperature and only 11 microvolts lower at liquid nitrogen. Schirber's scale was then shifted to agree with these two calibration points. The actual scale, which was obtained in this manner, is duplicated in Table 2 of the Appendix.

---

[1]Schirber, J. Ames, Iowa. The calibration of a gold-cobalt versus copper thermocouple. Private communication. 1958.

4. Electrical circuit

A standard dc method was used to obtain the electrical resistivity and Hall coefficient. The complete circuit is shown in Figure 4. Because the potential leads, made of constantan, had to be connected to copper leads it was feared that Seebeck emf's might produce fluctuations in output voltage. Thus the switch, standard resistor, and all lead connections were made inside an enclosed box placed near the top of the cryostat in an attempt to stabilize the voltages provided to the potentiometer.

For the remote control action necessary, a Ledex rotary switch positioner was mechanically coupled to a 5-wafer Leeds and Northrup type 31-3 twelve position rotary switch. The fifth wafer, which is not shown, served as a switch position indicator since it could apply voltage to one of a series of twelve pilot lights mounted on the control console. The switch was advanced a step at a time by the operator depressing the stepping button, also located on the control console.

Sample current was provided by a 6-volt automobile battery in series with a large variable resistor. The sample current was determined from the voltage across a standard resistor in series with the sample. Heater current was supplied by a 6 volt automobile battery in series with a variable resistor. Controls for both heater and sample current were located on the control console.

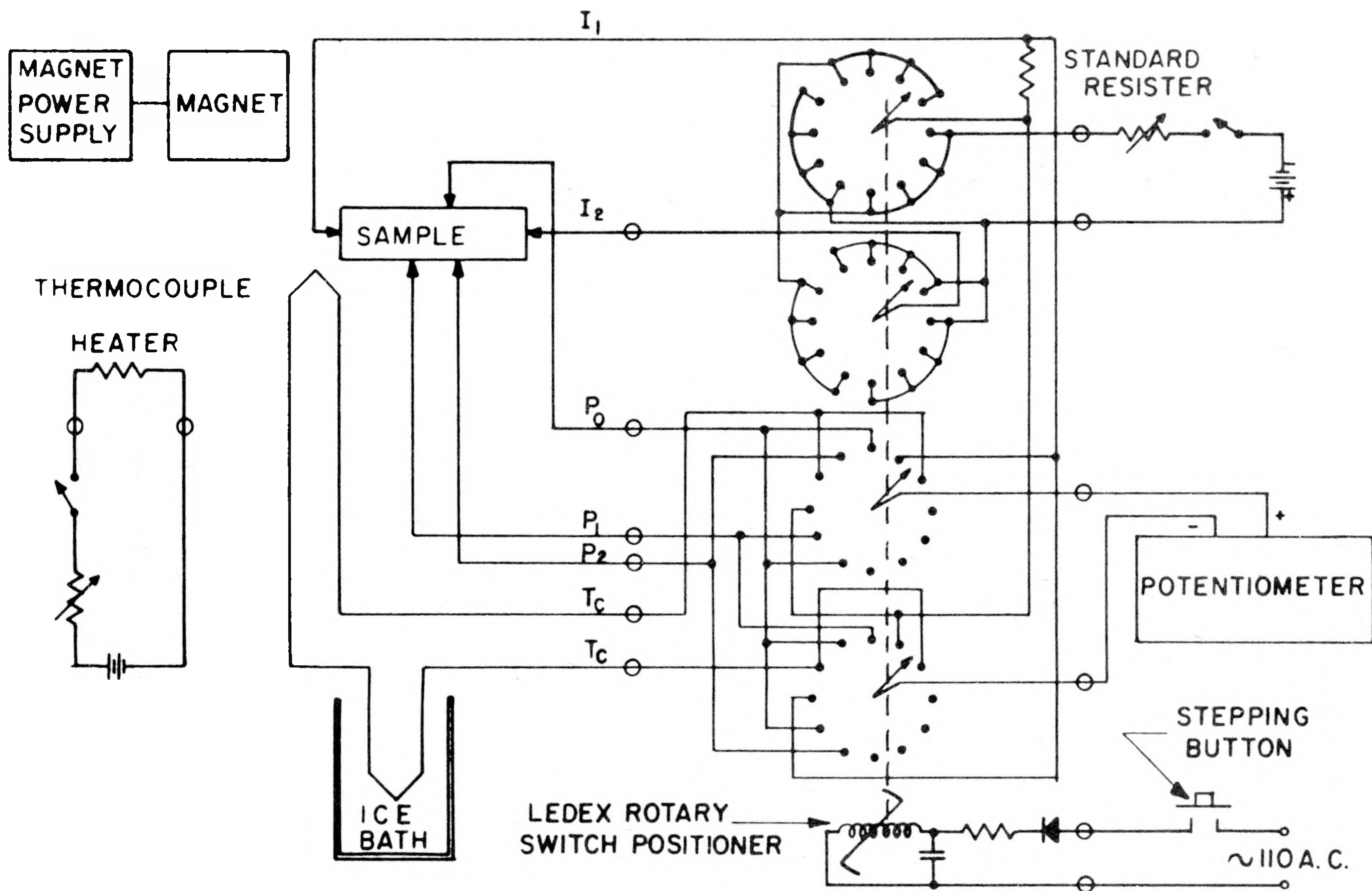

Figure 4. Electrical circuit

The magnetic field for this investigation was supplied by a Varian Electromagnet Model V-4012A fitted with tapered pole pieces having a 2.13-inch gap. Current for the magnet was supplied by a Varian Regulated Magnet power supply Model V-2100. A field of 10 kilogauss was used for the Hall effect measurements. The above mentioned combination provided a stability of 0.001 per cent at large fields. Repeatability, after the magnet had been cycled a few times, was better than one per cent.

All potential measurements were made with a Leeds and Northrup 7553 Type K-3 potentiometer. A Kintel Model 204A electronic galvanometer was used as a null detector. This combination provided an instrument error of one microvolt or less.

C. Electrical Measurements

1. Form of the data

Data were taken according to the sequence of the remote control switch shown in Figure 4. The sequence is as follows:

(1) Thermocouple, Tc;

(2) Plus sample current, +I;

(3) V_1 with plus sample current;

(4) V_2 with plus sample current;

(5) Thermocouple, Tc;

(6) Minus sample current, -I;

(7) V_1 with minus sample current;

(8) V_2 with minus sample current;

where V_1 is the potential between probes P_o and P_1 and V_2 is the potential between probes P_o and P_2. The above sequence was repeated three times - with no magnetic field, with plus field, and with minus field - for each point.

To reach equilibrium for each data point taken would be a costly waste of time. Instead the sample holder was deliberately disturbed from equilibrium by some transfer gas being pumped out of the sample chamber or the heater current being increased. A representative point, taken under the above dynamic conditions, is shown in Table 1. A series of these points were thus taken as a function of time, later to be plotted on larger graphs. At periodic intervals of time corresponding to the total time between points, values of all the variables were interpolated from the graphs. These values, including the thermocouple voltage, were then used to determine the Hall coefficient and resistivity at one specific temperature.

2. Check of Hall voltage linearity with magnetic field

The Hall voltage of the sample was measured as a function of the magnetic field strength at liquid helium and liquid nitrogen temperatures. The Hall voltage was found to be linear with magnetic field to the maximum field strength of 12.5

Table 1. A representative data point

Quantity measured	No H		+ H		- H	
	Voltage (μvolts)	Time (min.)	Voltage (μvolts)	Time (min.)	Voltage (μvolts)	Time (min.)
Tc	4376.6	226.38	4338.8	230.79	4308.4	234.46
+I	957.0	227.00	956.8	231.29	956.9	234.91
V_1 (+I)	2286.6	227.86	2655.2	231.68	1940.9	235.47
V_2 (+I)	559.0	228.34	244.9	232.13	884.7	236.15
Tc	4356.1	228.84	4324.1	232.68	4290.6	236.54
-I	957.1	229.23	957.0	233.03	957.6	236.99
V_1 (-I)	2244.8	229.57	2630.8	233.41	1924.2	237.34
V_2 (-I)	543.8	230.00	226.0	233.75	864.2	237.77

kilogauss.

3. Calculation of resistivity

The resistivity was computed by means of the formula

$$\rho = \frac{A}{dI}\left[\frac{V_1(+I,0H) + V_1(-I,0H) + V_2(+I,0H) + V_2(-I,0H)}{2}\right], \quad (1)$$

where ρ is the resistivity in ohm-cm, A is the average cross-sectional area in cm^2, d is the spacing between probes P_1 and P_2, and I is the sample current in amperes. Also the quantities in parenthesis behind the V's indicated the potential measurement was taken with a plus or minus sample current and either no, plus, or minus magnetic field. The four voltages

were added because the switch (Figure 4) reversed the lead potentials with the sample current to provide the potentiometer with the same polarity of voltage. This average of four voltages should have removed the effects of any slowly changing Seebeck emf's present in the measuring loop. The resistivities of sample B5-1 are tabulated in the Appendix, Table 3. A plot of these resistivities as a function of 1000/T is shown along with the Hall coefficient in Figure 5.

4. Calculation of Hall coefficient

The sample with its three probes, as well as the normal directions of current and magnetic field is shown in Figure 6. When this sample holder was used, probe P_o was always placed between probes P_1 and P_2. Since the IR drop between probes P_2 to P_o and P_o to P_1 was usually much larger than the Hall voltage produced, it dominated the polarity of V_1 and V_2. To facilitate rapid use of the potentiometer, the remote control switch was wired to present the same polarity of voltage to the potentiometer. The two sets of voltages shown in Figure 6, one set as a function of (+I) and the other set as a function of (-I), are each labeled with a sign to indicate how its polarity was treated by the potentiometer.

Treating V_1 as an example, and using the proper signs to take care of the switching arrangement, one would have the following equations according to Lindberg (9):

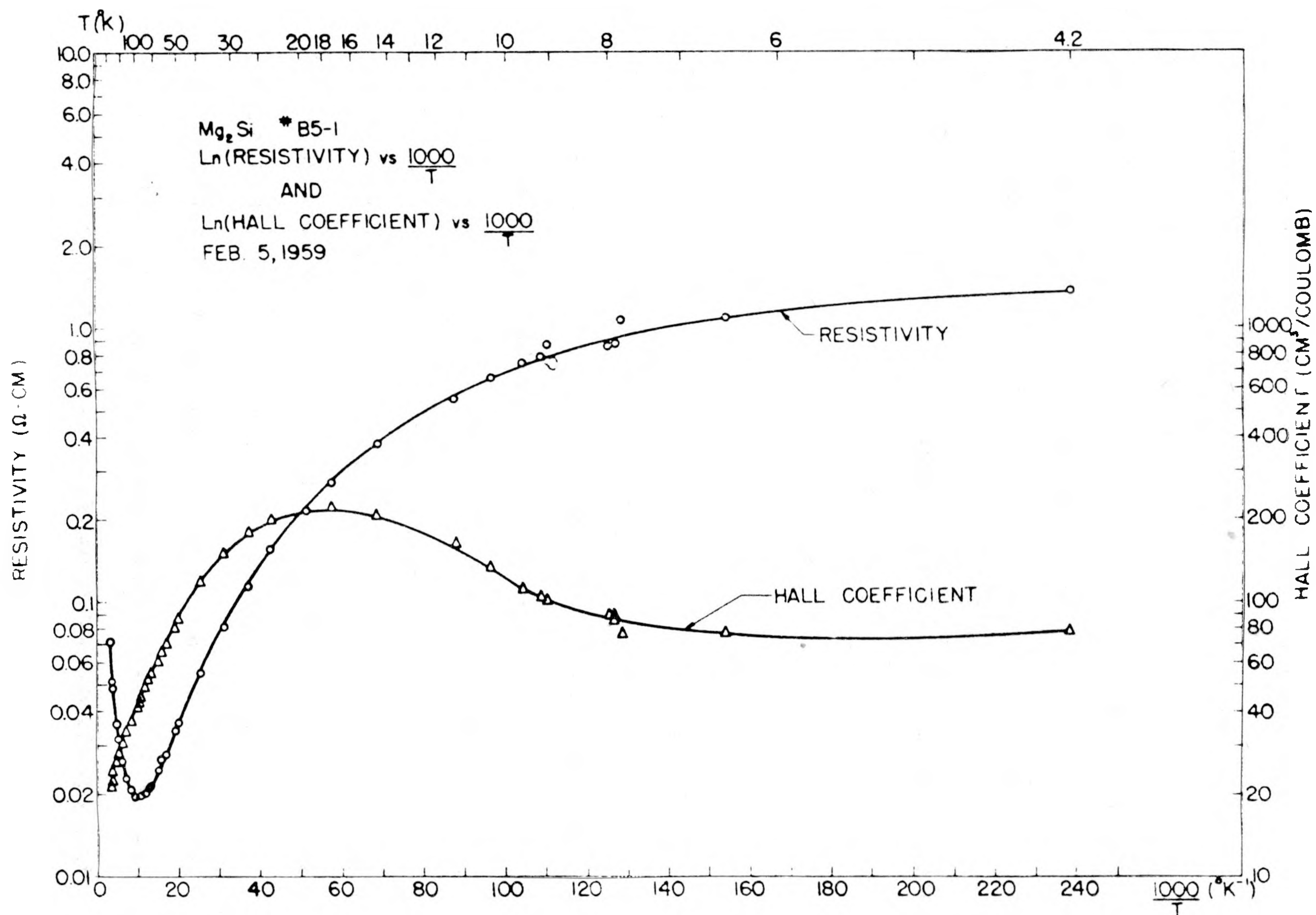

Figure 5. Hall coefficient and resistivity of sample B5-1 vs. 1000/T

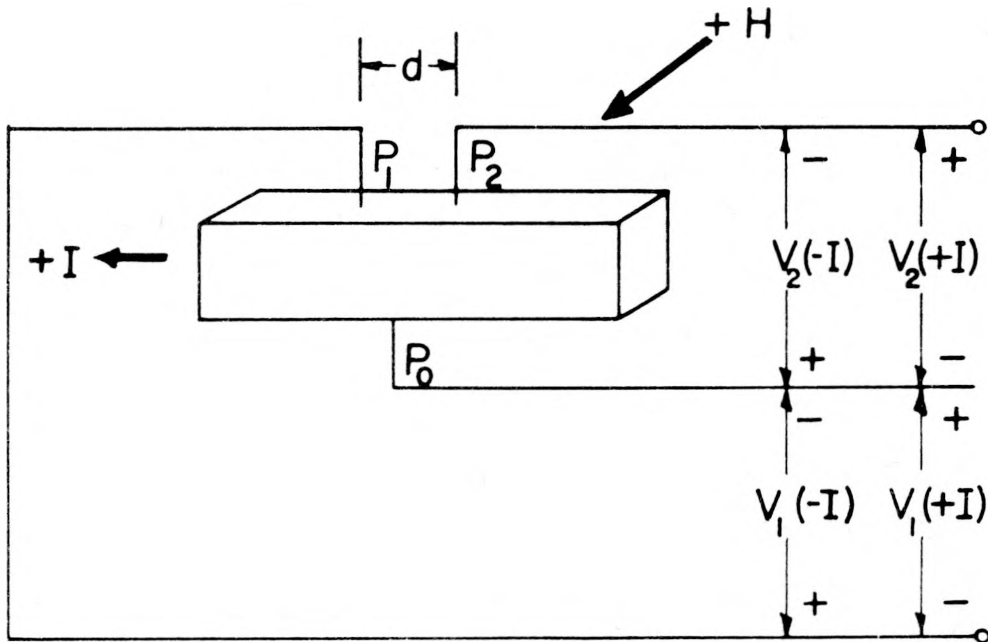

Figure 6. Orientation of sample and probes with respect to the magnetic field and current directions

$$V_1(+I, +H) = -V_H + V_{IR} + V_{MR} + V_T - V_E - V_N - V_{RL}, \quad (2)$$

$$V_1(+I, -H) = +V_H + V_{IR} + V_{MR} + V_T + V_E + V_N + V_{RL}, \quad (3)$$

$$V_1(-I, +H) = -V_H + V_{IR} + V_{MR} - V_T - V_E + V_N + V_{RL}, \quad (4)$$

$$V_1(-I, -H) = +V_H + V_{IR} + V_{MR} - V_T + V_E - V_N - V_{RL}, \quad (5)$$

where

V_H is the Hall voltage,

V_{IR} is the ohmic voltage,

V_{MR} is the additional ohmic voltage produced by magnetoresistance,

V_T is the Seebeck voltage in the measuring loop,

V_E is the Ettingshausen effect voltage,

V_N is the Nernst effect voltage,

V_{RL} is the Righi-Leduc effect voltage.

Combining Equations 2 to 5 properly one obtains

$$V_H + V_E = \frac{-V_1(+I,+H) + V_1(+I,-H) - V_1(-I,+H) + V_1(-I,-H)}{4} . \quad (6)$$

Treating V_2 in a similar manner yields

$$V_H + V_E = \frac{+V_2(+I,+H) - V_2(+I,-H) + V_2(-I,+H) - V_1(-I,-H)}{4} . \quad (7)$$

This method of measurement allows the determination of the sign and magnitude of the Hall coefficient according to the equation

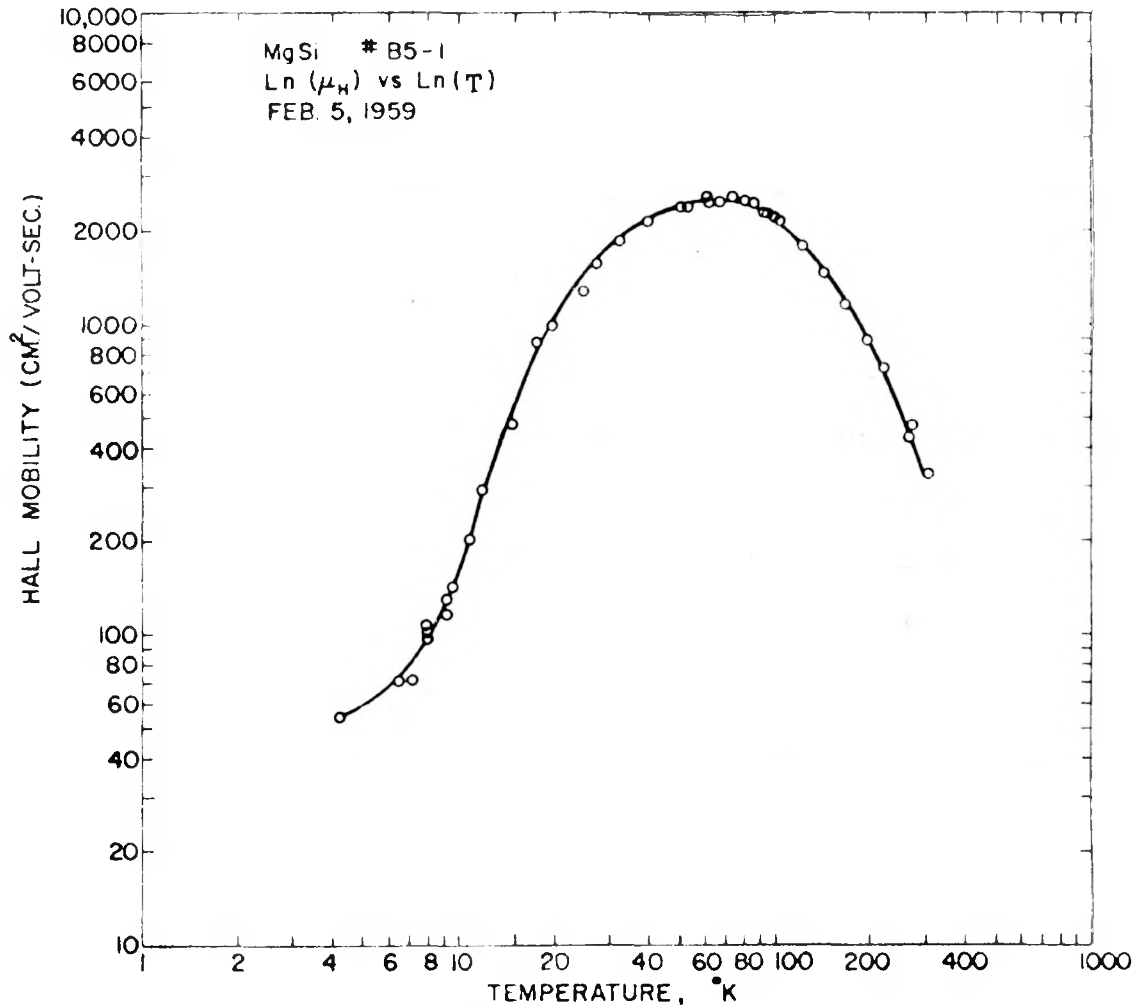

Figure 7. Hall mobility of sample B5-1 vs. temperature

$$R = \frac{t(V_H + V_E)}{IH} (10^8) , \qquad (8)$$

where R is the Hall coefficient in cm^3/coulomb, t is the thickness of the sample in cm, I is the sample current in amperes, and H is the magnetic field in gauss. Equation 8 shows that the influence of Ettingshausen effect voltage cannot be separated from the calculation of the Hall coefficient by a dc method of measurement. This effect will be discussed further in Section D.

It should be pointed out that Equations 6 and 7 each give an independent measurement of the Hall voltage. When the probes were placed on the sample, probe P_o was lined up more closely with probe P_2. It was assumed at that time that V_2 would therefore give the more reliable and more stable Hall voltage due to the smaller IR drop included. However, calculation of Hall voltage by V_1 and V_2 over the entire temperature range revealed very little scatter in either measurement. Thus the two Hall coefficients for each temperature were averaged and entered into Table 3 of the Appendix. Also the absolute value of the averaged Hall coefficient is plotted versus 1000/T along with the resistivity in Figure 5. The Hall coefficient of this sample remained negative through the entire temperature range considered, indicating an n-type impurity.

D. Errors

1. Resistivity

The effect of voltage measurement errors on resistivity caused by unstable Seebeck emf's, instrument error, and interpolation of voltage versus time plots was estimated to be less than one per cent. The error in the determination of sample current was likewise less than one per cent. The dominant source of error was that of cross-sectional area caused by non-rectangularity of the sample, chips and shallow scratches, and travelling microscope error. This error was calculated to be as large as 12 per cent. Another large source of error was the determination of probe spacing, d, due chiefly to the thickness of the probes and the short spacing. This error could be as much as 8 per cent.

The total effect of all errors amounted to a 15 per cent error in resistivity measurement. Fortunately, this error affects only the magnitude and not the temperature dependence of resistivity.

2. Hall coefficient

The sample thickness dimension had an error introduced into it by chips, scratches, irregular geometry, and traveling microscope error. Its total magnitude was estimated at 7 per cent. Sample current, as stated previously, was less than

one per cent. Magnetic field error was about one per cent.

The error introduced into the Hall coefficient calculation due to the Hall voltage has three contributions:

(1) voltage measurement errors;

(2) sample geometry; and

(3) Ettingshausen effect voltage.

Voltage measurement errors play a bigger role in the Hall voltage than in resistivity because large voltages are subtracted to obtain small differences. The maximum error due to this contribution is estimated at 3 per cent. Isenberg, _et al_. (6) computed the short circuiting effect of area contact current probes on the Hall voltage. The length-to-width ratio of this sample was 4.1, which means according to Isenberg's table, that no corrections are necessary.

The last uncertainty in Hall voltage is caused by the inability of this measuring technique to separate Hall voltage from Ettingshausen effect voltage. Johnson and Shipley (7) in a theoretical treatment of semiconductors have given equations relating the adiabatic Hall coefficient to the isothermal Hall coefficient. A survey of this paper shows that the per cent change in the Hall coefficient owing to the Ettingshausen effect coefficient is proportional to σ/K, where σ is the electrical conductivity and K is the thermal conductivity. For a germanium sample with similar impurity concentration to that of the sample under investigation in this

research, the largest contribution of Ettingshausen effect to the Hall coefficient was 2 per cent. This error was computed by Johnson and Shipley (7) at 300°K on the basis of σ= 1000 mho/cm. and K = 0.6 watt/°K-cm. for germanium. For the Mg_2Si sample in this research, the largest value of electrical conductivity measured was σ= 50 mho/cm. No thermal conductivity data for Mg_2Si are available, but Busch and Schneider (1) give the thermal conductivity for Mg_2Sn at 300°K as approximately 0.084 watts/°K-cm. Using these two numbers for our comparison to Johnson and Shipley's germanium sample, one arrives at the maximum contribution of Ettingshausen effect to Hall coefficient as less than one per cent. Thus, it seems that the Ettingshausen effect does not contribute appreciably to the measurements taken in this work.

A consideration of all factors affecting this measurement of Hall coefficient leads to an overall error of 9 per cent. This error is also one of magnitude and independent of temperature.

3. Temperature

The thermocouple was cemented to a 0.010-inch thick copper strip, used for the fixed current probe, at a distance of about 3/8 inch from the point where the sample touched the strip. This copper strip, which is called the fixed current probe in Figure 3, had to be made of commercial grade copper

because of the necessary right angle bend in it. Thus, there was actually a poor thermal path between the sample and thermocouple. It was not known until this run whether this would affect temperature measurements.

To determine the linearity of Hall voltage with magnetic field at liquid helium temperature, the sample holder was allowed to reach equilibrium with 2 milliamperes of sample current and less than one atmosphere of transfer gas surrounding it. Seven points were taken, all of which yielded the same value of resistivity. Everything else was left unchanged but the sample current was raised to 8 milliamperes and six points were taken. These also yielded a constant value of resistivity. In all cases, the thermocouple continued to indicate a liquid helium temperature. However, there was a marked decrease in resistivity in the second case, indicating that the sample had actually increased in temperature, while the thermocouple had been unable to detect the change. When the run was completed, resistivities were plotted versus thermocouple temperature. This curve was extrapolated and the 2 milliampere point was found to be 2.3°K lower than the 8 milliampere point. This seems very reasonable, since the 8 milliampere point was dissipating 16 times the sample power that the 2 milliampere point had been dissipating.

A correction was obviously needed for the temperature lag

produced by the sample holder. For lack of anything better, the 2 milliampere point was assumed to be taken at 4.2°K and correction quantities were added to other thermocouple temperatures according to

$$(2.3°K)\left[\frac{\text{sample power dissipated at the point in question}}{\text{sample power dissipated at the 8 ma. point}}\right]. \quad (9)$$

Because a nearly constant value of sample current was used for the remaining points and because the resistivity decreased rapidly from the 4.2°K point, the size of the correction term also diminished rapidly as temperature increased.

The thermocouple itself had an inherent error caused by the inhomogeneities of the gold-cobalt wire and thermal gradients near the cryostat top. One could cause the thermocouple reading to change a few microvolts by warming the cryostat cap with the hand. Referring to Table 2 of the Appendix, one sees that this type of error is more serious at low temperatures than at high temperatures. An estimate of thermocouple error would be ± 1°K at liquid helium temperature, decreasing in proportion to the thermoelectric power of the thermocouple. In this manner, the thermocouple error would be ± 0.2°K at room temperature.

III. ANALYSIS OF THE RESULTS

A. Hall Coefficient

A qualitative look at the Hall coefficient versus 1000/T curve, Figure 5, reveals a low temperature maximum with a decrease to what seems to be a saturation value below 7°K. A preliminary search of existing literature revealed similar curves for heavily doped germanium and silicon samples. These curves have been interpreted as manifestations of an impurity band conduction phenomenon. A summary article by E. M. Conwell (3), who puts the matter of impurity band conduction on a more firm theoretical basis, will be referred to often in the analysis of these data.

The ground state Bohr radius of a donor impurity in a semiconductor would be

$$r^* = \frac{\epsilon \hbar^2}{e^2 m^*}, \tag{10}$$

according to Kittel (8, p. 356), where

r^* = Bohr radius in a semiconductor,

ϵ = dielectric constant of the semiconductor material,

$\hbar$ = $1.054(10^{-27})$ erg-sec,

e = $4.8(10^{-10})$ esu,

m^* = effective electron mass, with spherical energy surfaces assumed.

At low impurity concentrations, these hydrogen-like wave func-

tions are separated by many Bohr radii, and therefore allow discrete levels at values of energy referred to in normal semiconductor work as impurity levels. If the atomic polyhedra surrounding each impurity are approximated by spheres of radius r_s, a cellular method gives

$$\left(\frac{4\pi}{3}\right) r_s^3 = \frac{1}{N_I} \qquad (11)$$

where N_I is the number of majority carriers per cm^3.

Conwell (3), neglecting excited levels, predicts the advent of an impurity band at $r_s = 5r^*$ and the merging of the impurity band with the conduction band at $r_s = r^*$, where r^* is the Bohr radius referred to in Equation 10. To utilize this last equation in computing the Bohr radius for Mg_2Si the value $m^* = 0.46$ m, which Morris, et al. (11) determined from intrinsic measurements of Mg_2Si, was used. The dielectric constant ϵ was determined in the following way. Moss (12) noted that in semiconductors $\Delta E_o \epsilon^2$ is a constant, where ΔE_o = gap energy at 0°K. An average of eight values quoted by Madelung (10) in his review article on semiconductors gives $\Delta E_o \epsilon^2 = 155$, although the relationship is not understood theoretically. Using Morris' (11) value of 0.78 ev for ΔE_o, one obtains $\epsilon = 14$ for Mg_2Si. Substituting the above constants into Equation 10, one obtains $r^* = 1.618(10^{-7})$ cm for the Bohr radius of the n-type impurity in Mg_2Si.

Using Conwell's criterion for impurity band conduction

and Equation 11, the following limits on impurity concentration are reached for Mg_2Si:

$$4.5 \times 10^{17}\ cm^{-3} \leq N_I \leq 5.6 \times 10^{19}\ cm^{-3}. \quad (12)$$

Since the ionization energy of the impurity level is considerably less than the width of the band gap, all the impurity levels will be ionized before the sample becomes intrinsic. Since each ionized impurity level contributes one charge carrier, the value of the carrier concentration at temperatures just below intrinsic behavior is an indication of the density of impurity levels. Because both n- and p-type impurities exist in semiconductors, compensation takes place. The excess of donor impurities over acceptor impurities is given by the equation

$$N_D - N_A = - \frac{(3\pi/8)}{R_{300°}}, \quad (13)$$

where N_D is the concentration of donor levels, N_A is the concentration of acceptor levels, and $R_{300°}$ is the Hall coefficient at 300°K. For the sample investigated in this work $(N_D - N_A) = 3.5 \times 10^{17}\ cm^{-3}$. A rough comparison to Equation 12 seems to indicate that the criterion for weak impurity band conduction has been met.

Most of the samples of doped germanium shown in Conwell's article (3) are in the strong impurity band carrier concentration region. The carrier concentration minimum for Conwell's

sample 74, however, is at the same temperature and about the same depth as the Hall coefficient peak of this Mg_2Si sample shown in Figure 5. Conwell's theory likewise predicts very weak impurity band effects in her sample 74.

B. Hall Mobility

Conwell (3) gives equations for the low-field Hall constant

$$R = \frac{n_1\mu_{1H}\mu_1 + n_2\mu_{2H}\mu_2}{(n_1\mu_1 + n_2\mu_2)^2} = \frac{\langle\mu_H\mu\rangle}{\langle\mu\rangle^2}\frac{1}{(n_1 + n_2)} \qquad (14)$$

and Hall mobility as:

$$\mu_H = \frac{n_1\mu_{1H}\mu_1 + n_2\mu_{2H}\mu_2}{n_1\mu_1 + n_2\mu_2} = \frac{\langle\mu_H\mu\rangle}{\langle\mu\rangle}, \qquad (15)$$

where

R = Hall coefficient,

n_1 = conduction band carrier concentration,

μ_{1H} = conduction band Hall mobility,

μ_{2H} = impurity band Hall mobility,

μ_1 = conduction band mobility,

μ_2 = impurity band mobility,

μ_H = total Hall mobility, and

μ = total mobility.

Assuming μ_1/μ_2, denoted by b, is independent of temperature, and $\mu_H/\mu = 1$, Conwell (3) finds that Equation 14 yields the

important result,

$$\frac{R_{300°}}{R_{max}} = \frac{4b}{(b + 1)^2} , \qquad (16)$$

where $R_{300°}$ is the Hall coefficient at 300°K and R_{max} is the Hall coefficient at its peak value. The systematic heightening of the Hall coefficient peak as well as its shift to lower temperatures with a decrease in impurity concentration is summed up quantitatively in Equation 16. This equation yields a value of $b = 38$ for the Mg_2Si sample of this research. This large value means an extremely low impurity band mobility, further corroborating the prediction of weak impurity band conduction.

The Hall mobility curve for the sample of Mg_2Si measured in this work is shown in Figure 7. Its temperature dependence of T^{-22} in the temperature range of 100° - 300°K has been suitably explained by Morris, _et al_. (11), who used a combination of optical mode and ionized impurity scattering to fit this region quite well for similar single crystals of Mg_2Si. The next lower temperature region seems to be one of gradual transition from a negative to a positive power temperature dependence. Centered approximately at 15°K is a linear region in which the Hall mobility varies as $T^{3.1}$.

One sees from Figure 5 that the Hall coefficient reaches a maximum and begins to decrease rapidly with a decrease in

temperature at 17°K. If one believes an impurity band exists, these Hall data mean that the carriers are being rapidly transferred from the conduction band to the impurity band in this temperature region. However, invoking an impurity band also allows the use of Equation 15 for the Hall mobility. The ratio $\mu_1/\mu_2 = 38$ has been determined so that in the vicinity of 17°K one would expect a steep decrease of Hall mobility with a decrease in temperature as the sample conduction begins to be dominated by the impurity band. The above argument seems to be more satisfactory than normal conduction band scattering theories, since the strongest temperature dependence they predict is $T^{1.5}$ due to ionized impurities.

C. Impurity Level

It had been decided in Sections A and B that the sample of Mg_2Si measured for this investigation had an impurity concentration which caused it to have weak impurity band conduction. Since this type of conduction would imply a very narrow impurity band centered around what would be normally called an impurity level, it should be possible to determine the activation energy of this level with some meaning. At a few hundred degrees below the onset of intrinsic conduction, the activation of these levels is the main cause of the change of Hall coefficient as a function of temperature.

Kittel (8, p. 360) lists the following equation as an

approximation to the variation of conduction band carrier concentration as a function of temperature:

$$n = (2N_d)^{\frac{1}{2}} \left(\frac{2\pi KTm^*}{h^2}\right)^{3/4} \exp\left(-\frac{E_d}{2KT}\right) , \tag{17}$$

where

n = conduction band concentration of electrons,

N_d = concentration of donor impurities,

K = Boltzmann's constant = $1.38(10)^{-16}$ erg $(°K)^{-1}$,

T = temperature (°K),

m^* = electron effective mass,

h = Planck's constant $6.62(10)^{-27}$ erg sec, and

E_d = activation energy of donor impurities.

If one assumes no impurity band carriers, then Equation 14 reveals n is inversely proportional to the Hall coefficient. When the last proportionality is substituted into Equation 17 it may be seen that a plot of log $(RT^{3/4})$ vs. $1/T$ should give a straight line with slope $E_d/2K$. A plot was made for these data and can be seen in Figure 8.

The plot in Figure 8 consists of a negative slope region at high and low temperatures with a positive slope region between. A best-fit line was passed through the eight points appearing between 40 - 80°K in the positive slope region. The slope of this line yielded a value of E_d = 0.0045 ev.

As the temperature decreases below 40°K one sees the gradually widening deviation of the points from the straight

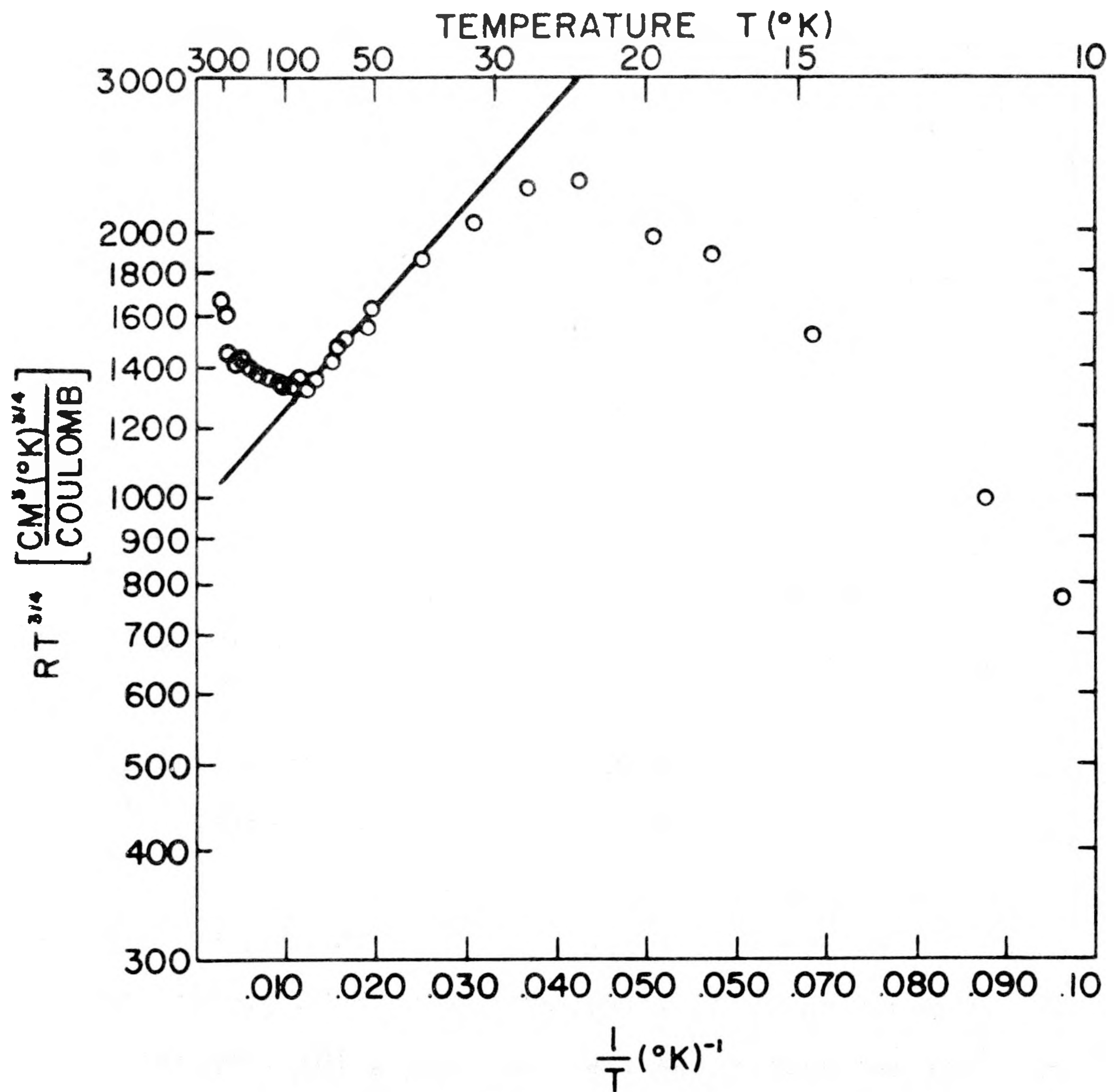

Figure 8. $RT^{3/4}$ vs. 1/T for sample B5-1

line drawn in Figure 8 until the points begin to approach a negative slope region. This deviation may be almost entirely due to the effect of impurity band carriers.

At the higher temperature end of the plot in Figure 8 one may also notice a negative slope deviation from the straight line used to determine the activation energy. To give a possible explanation of this, one must realize that Equation 17 is an approximation which Kittel (8, p. 360) claims rests on the validity of the following inequality:

$$\frac{2N_d}{(2\pi m^*KT/h^2)^{3/2}} \exp\left(\frac{E_d}{KT}\right) \gg 1 \ , \qquad (18)$$

where

N_d = donor impurity concentration,

m^* = electron effective mass,

K = Boltzmann's constant = $1.38(10)^{-16}$ erg $(°K)^{-1}$,

T = temperature (°K),

h = Planck's constant = $6.62(10)^{-27}$ erg sec, and

E_d = activation energy of the impurity level.

If the value E_d = 0.0045 ev obtained from these data is assumed to be correct, a calculation of the quantity on the left of Equation 18 at a temperature of 80°K yields the value 2.8. One can easily see that increasing the temperature rapidly decreases the value of the quantity on the left of Equation 18 to less than 2.8 while decreasing the temperature will have quite the opposite effect. The certain failure to

meet the requirement of Equation 18 may be the cause of the negative slope region at higher temperatures. How this value of 2.8 at 80°K actually effects the determination of E_d is not known.

D. Impurity Compensation

In the previous sections arguments have been presented for belief that weak impurity-band conductivity has been observed in this investigation. For weak impurity band conductivity of the type just mentioned, Conwell (3) treats each electron as definitely associated with an impurity atom. She then considers a crude theory in which electron conduction occurs by the process of quantum-mechanical tunneling of potentials. Applying this theory to highly compensated samples at 4°K, she arrives at her Equation 7. When the appropriate constants for the Mg_2Si sample of this work are substituted into her equation, one obtains

$$\rho = 2.83 \times 10^{-4} \left(\frac{N_D}{N_A}\right) \exp\left(\frac{2r_s}{r^*}\right) , \qquad (19)$$

where

ρ = resistivity at 4°K (r-cm),

N_D = donor impurity concentration,

N_A = acceptor impurity concentration,

$r_s = \left[\frac{1}{(4\pi/3)N_D}\right]^{1/3}$, the radius based on the cellular method, and

r^* = Bohr radius of the electrons associated with the donor impurity.

The equation similar to Equation 19 was used by Conwell (3) to estimate the amount of compensation in three germanium samples, but was unsuccessful in predicting the temperature variation of their resistivity. In like manner for this sample of Mg_2Si, $\rho = 1.36 \Omega$-cm and $r^* = 1.618(10)^{-7}$ cm were inserted into Equation 19. Since r_s is a function of N_D, an iterative method was used to solve the equation.

The final solution of Equation 19 for the sample of this work yielded $N_A/N_D = 0.5$, meaning that approximately 50 ± 25 per cent compensation existed.

IV. LITERATURE CITED

1. Busch, G. and Schneider, M. Heat conduction and semiconductors. Physics 20: 1084-1086. 1954.

2. Chelton, D. B. and Mann, D. B. Cryogenic data book. U. S. Atomic Energy Commission Report UCRL-3421. (California. Univ., Berkeley. Radiation Lab.) May 15, 1956.

3. Conwell, E. M. Impurity band conduction in germanium and silicon. Phys. Rev. 103: 51-61. 1956.

4. Frederikse, H. P. R., Hosler, W. R., and Roberts, D. E. Electrical conduction in magnesium stannide at low temperatures. Phys. Rev. 103: 67-72. 1956.

5. Fuschillo, N. A low temperature scale from 4° to 300°K. in terms of a gold-cobalt versus copper thermocouple. J. Phys. Chem. 61: 644-649. 1957.

6. Isenberg, I., Russell, B. R., and Greene, R. F. Improved method of measuring Hall coefficients. Rev. Sci. Instr. 19: 685-688. 1948.

7. Johnson, V. A. and Shipley, F. M. The adiabatic Hall effect in semiconductors. Phys. Rev. 90: 523-529. 1953.

8. Kittel, C. Introduction to solid state physics. 2nd ed. New York, N. Y., John Wiley and Sons. 1956.

9. Lindberg, Olof. Hall effect. Proc. Inst. Radio Engrs. 40: 1414-1419. 1952.

10. Madelung, O. H. Handbuch der physik. Vol. 20. Berlin, Springer Verlag. 1957.

11. Morris, R. G., Redin, R. D., and Danielson, G. C. Semiconducting properties of Mg_2Si single crystals. Phys. Rev. 109: 1909-1915. 1958.

12. Moss, T. S. Photoconductivity in the elements. New York, N. Y., Academic Press. 1952.

13. Powell, R. L. and Blanpied, W. A. Thermal conductivity of metals and alloys at low temperatures. National Bureau of Standards Circular 556: 58-59. 1954.

14. Whitsett, Charles R. Electrical properties of magnesium silicide and magnesium germanide. Unpublished Ph.D. Thesis. Ames, Iowa, Iowa State College Library. 1955.

15. Winkler, U. Die elektrishen Eigenschaften der intermetallischen Vergindungen Mg_2Si, Mg_2Ge, Mg_2Sn und Mg_2Pb. Helv. Phys. Acta. 28: 633-666. 1957.

V. APPENDIX

Table 2. Gold-cobalt vs. copper thermocouple calibration used for this work

T(°K)	EMF (μvolts)	Δ (μvolts)	T(°K)	EMF (μvolts)	Δ (μvolts)
4.0	9339	6	28.0	9032	40
5.0	9333	7	30.0	8992	43
6.0	9326	7	32.0	8949	45
7.0	9319	8	34.0	8904	47
8.0	9311	8	36.0	8857	49
9.0	9303	9	38.0	8808	51
10.0	9294	10	40.0	8757	51
11.0	9284	10	42.0	8706	52
12.0	9274	10	44.0	8654	55
13.0	9264	11	46.0	8599	56
14.0	9253	12	48.0	8543	57
15.0	9241	13	50.0	8486	148
16.0	9228	13	55.0	8338	152
17.0	9215	13	60.0	8186	157
18.0	9202	14	65.0	8029	161
19.0	9188	15	70.0	7868	165
20.0	9173	31	75.0	7703	62
22.0	9142	35	77.0	7641	100
24.0	9107	36	80.0	7541	169
26.0	9071	39	85.0	7372	174

Table 2. (Continued)

T(°K)	EMF (μvolts)	Δ (μvolts)	T(°K)	EMF (μvolts)	Δ (μvolts)
90.0	7198		170.0	4146	
		180			399
95.0	7018		180.0	3747	
		183			400
100.0	6835		190.0	3347	
		185			400
105.0	6650		200.0	2947	
		185			400
110.0	6465		210.0	2547	
		187			402
115.0	6278		220.0	2145	
		189			403
120.0	6089		230.0	1742	
		190			403
125.0	5899		240.0	1339	
		190			400
130.0	5709		250.0	939	
		190			404
135.0	5519		260.0	535	
		193			404
140.0	5326		270.0	131	
		198			405
145.0	5128		280.0	-274	
		197			404
150.0	4931		290.0	-678	
		389			404
160.0	4542		300.0	-1082	
		396			

Table 3. Resistivity and Hall coefficient of sample B5-1

Temp. T (°K)	$\frac{1000}{T}$ (°K)$^{-1}$	Resistivity (ohm-cm)	Hall coefficient, R (cm^3/coulomb)	Hall mobility H (cm^2/volt-sec.)
4.2	238.0	1.360	76.0	55.8
6.5	153.8	1.067	75.6	70.8
7.8	128.2	1.061	75.4	70.9
8.0	125.0	0.859	88.1	102.7
7.9	126.6	0.873	87.2	99.8
7.9	126.6	0.864	93.2	108.0
9.1	110.0	0.790	101.0	117
9.2	108.7	0.783	102.5	131
9.6	104.1	0.747	110.0	147
10.4	96.2	0.658	132.5	201
11.4	87.7	0.553	161.0	291
14.6	68.5	0.379	204.0	438
17.4	57.4	0.272	220.0	808
19.6	51.0	0.215	212.0	986
23.6	42.4	0.157	200.0	1274
27.1	36.9	0.114	178.0	1560
32.4	30.9	0.0804	150.0	1865
39.5	25.3	0.0551	118.0	2140
50.5	19.8	0.0363	86.0	2370
52.3	19.1	0.0340	80.0	2350
60.3	16.6	0.0278	69.6	2505
63.6	15.7	0.0268	65.8	2455
67.1	14.9	0.0245	60.7	2480
76.8	13.1	0.0212	54.3	2560
85.6	11.7	0.0200	48.6	2430
93.1	10.8	0.0197	45.0	2285
99.3	10.1	0.0195	42.6	2185
80.0	12.5	0.0209	51.3	2455
94.0	10.6	0.0199	44.4	2230
100.0	10.0	0.0195	42.4	2170
104.0	9.6	0.0194	41.6	2145
123.0	8.1	0.0206	36.8	1785
143.1	7.0	0.0228	33.3	1460
166.6	6.0	0.0262	30.2	1153
194.6	5.1	0.0316	27.9	883

Table 3. (Continued)

Temp. T (°K)	$\frac{1000}{T}$ (°K)$^{-1}$	Resistivity (ohm-cm)	Hall coefficient, R (cm^3/coulomb)	Hall mobility H (cm^2/volt-sec.)
264.0	3.8	0.0489	22.2	433
209.0	4.8	0.0358	25.9	723
269.6	3.7	0.0506	24.1	476
300.0	3.3	0.0717	23.2	325